Electromagnetic Scattering using a Plane Wave $\boldsymbol{H}(\mathrm{curl})$ Conforming Finite Element Method

P.D. Ledger

Research Report No. 2004-13
October 2004

Seminar für Angewandte Mathematik
Eidgenössische Technische Hochschule
CH-8092 Zürich
Switzerland

Electromagnetic Scattering Simulations using a Plane Wave $\boldsymbol{H}(\mathrm{curl})$ Conforming Finite Element Method

P.D. Ledger

Seminar für Angewandte Mathematik
Eidgenössische Technische Hochschule
CH-8092 Zürich
Switzerland

Research Report No. 2004-13 October 2004

Abstract

This paper describes a two dimensional edge element discretisation of Maxwell's equations in which the standard lowest order basis functions for the $\boldsymbol{H}(\mathrm{curl})$ space are augmented by plane wave expansions. The aim is to improve the accuracy of the underlying low order scheme for electromagnetic scattering problems. A method to determine the directions of the plane waves on edges inside the mesh is proposed in which the condition number of the global matrix is controlled. Improvements in the calculation of the scattering width distribution lead to substantial improvements in accuracy. A range of two–dimensional scattering examples are included and comparisons with a *hp*–version code are undertaken.

1 Introduction

The aerospace industry is interested in electromagnetic scattering problems where the wavelength of the wave is short compared to the length of the scatterer. This problem is made more complex as the scatterer may contain multi–materials and have many sharp corners. In fact, the primary interest lies in the accurate evaluation of the scattering width distribution, which can be computed directly as an output of the scattering problem. This output represents the far field pattern of the scatterer and may be used for the radar detection of civilian and military vehicles.

The $\boldsymbol{H}(\mathrm{curl})$ conforming finite elements first introduced by Nédélec [27, 28, 29] are well suited to such problems as these elements can readily handle material interfaces and boundary conditions. In addition, the spurious modes which are known to occur when components of the field variables are discretised by nodal finite elements do not occur with $\boldsymbol{H}(\mathrm{curl})$ conforming finite elements [31, 26]. Within the engineering community, these elements have become better known as edge elements. This is in part due to the fact that the lowest order $\boldsymbol{H}(\mathrm{curl})$ conforming approximation has a degree of freedom associated with each edge of the element.

Unfortunately the standard lowest order $\boldsymbol{H}(\mathrm{curl})$ conforming elements are known to have bad dispersive properties which make them unsuitable for using in problems when the wavelength is small [33, 2, 1]. As this is exactly the problem in which the aerospace industry is interested in, then this makes the application of low order elements inappropriate. Considerable success at minimising dispersion was obtained when hp–version $\boldsymbol{H}(\mathrm{curl})$ conforming finite elements were used to discretise Maxwell's equations [19, 17, 21, 18]. Indeed, for meshes composed of squares one can directly quantify the dispersion for a given mesh spacing h and polynomial order p [2, 1]. An interesting approach which attempts to minimise the dispersive behaviour for all wave directions on the stencil resulting from the lowest order square edge element was proposed in [12]. The idea for this follows on from the work of Babuska, Sauter and coworkers [5, 4] who proposed the so called generalised finite element method for the Helmholtz equation. In this approach they were able to eliminate the dispersion for one–dimensional problems and minimise it for two–dimensional problems. This was achieved by modifying the H^1 finite element stencil for a mesh composed of uniformly sized square elements. The approach presented in [12] considers Maxwell wave propagation and scattering problems, for both cases accurate results were obtained with the modified stencil.

Using meshes consisting only of square elements places a restriction on the type of scatterer that can considered. In this work we explore an alternative approach for solving electromagnetic scattering problems, without this restriction. The new procedure enriches the lowest order $\boldsymbol{H}(\mathrm{curl})$ conforming space with a series of plane wave expansions. The idea of supplementing standard $\boldsymbol{H}(\mathrm{curl})$ conforming elements with expansions of plane waves comes from the work of Melenk and Babuska [22, 3] who developed the partition of unity finite element method in which the underlying finite element space was enriched by additional knowledge about the solution. In this case, as in the later work of Bettess *et. al.* [16, 15], one of the main areas of interest was the solution of the Helmholtz equation and in–common with our approach the enrichment was through expansions of plane waves. The use of plane wave expansions makes an attractive choice as once the directions of the plane waves are correctly selected, the dispersion problems associated with standard elements become irrelevant.

What we describe in this report is an extension of our initial investigation [20] which considered wave propagation problems with Neumann boundary conditions. In this work, we shall extend this approach to two–dimensional scattering problems in which Dirchlet and Neumann boundary conditions can be applied and multi–material properties can be considered. In common with all domain based solvers for scattering problems, we require a method to truncate the otherwise infinite domain. Suitable candidates for this are absorbing boundary conditions [6], infinite elements [8, 10], coupling with boundary integral techniques [11] or a through application of an absorbing sponge layer [7]. In this work, the truncation will be accomplished by the perfectly matched layer (PML) approach of Berenger [7]. We adopt this approach due to its ease of implementation and the success that was previously obtained when it was used with hp–version $\boldsymbol{H}(\mathrm{curl})$ conforming elements for scattering problems [17, 19, 21, 18].

The presentation of the material in this report proceeds as follows: In Section 2 the mathematical formulation of the problem will be stated together with an appropriate weak variational statement. Section 3 introduces the far field condition used to truncate the infinite domain together with the approximate weak variational statement of the problem. The plane wave $\boldsymbol{H}$(curl) conforming quadrilateral and triangular elements together with the necessary convairant transformation required for curvilinear elements is described in Section 4. In Section 5 some details of the computational procedure are described including how the directions of the plane waves may be chosen on Dirchlet and interior edges and how the scattering width output can be accurately evaluated. Section 6 gives a selection of numerical examples which demonstrate the computational performance of the proposed procedure. Examples with and without analytical solutions are undertaken and comparisons are made with a *hp* approach [17, 19, 21, 18].

2 Problem formulation

Let us consider Maxwell's equations expressed in the frequency domain for a source free medium

$$\text{curl}\,\boldsymbol{E} = -\mathrm{i}\mu\omega\boldsymbol{H} \qquad \text{curl}\,\boldsymbol{H} = \mathrm{i}\epsilon\omega\boldsymbol{E} \tag{1}$$

where $\boldsymbol{E}$ and $\boldsymbol{H}$ are the electric and magnetic field intensity vectors, ϵ and μ are the relative material parameters, the frequency is such that $\omega^2 > 0$ and $\mathrm{i}^2 = -1$. It is convenient to introduce a splitting of the electric and magnetic fields

$$\boldsymbol{E} = \boldsymbol{E}^s + \boldsymbol{E}^i \qquad \boldsymbol{H} = \boldsymbol{H}^s + \boldsymbol{H}^i \tag{2}$$

where the superscript i refers to the incident component and the superscript s to the scattered. The incident fields are chosen so as to satisfy Maxwell's equations in free space

$$\text{curl}\,\boldsymbol{E}^i = -\mathrm{i}\omega\boldsymbol{H}^i \qquad \text{curl}\,\boldsymbol{H}^i = \mathrm{i}\omega\boldsymbol{E}^i \tag{3}$$

where the material properties in free space have been normalised to unity. We wish to restrict consideration to two–dimensional problems expressed in Cartesian coordinates $O(x, y)$ in which the electric field has two components $\boldsymbol{E} = (E_x, E_y)^T$ and the magnetic field has only the component H_z (z direction into the page). The curl of a two dimensional vector field should be interpreted as $\text{curl}\,\boldsymbol{E} = \frac{\partial E_y}{\partial x} - \frac{\partial E_x}{\partial y}$. We shall consider perfect conducting scatterers with possible dielectric coatings. In the case of a perfect magnetic conductor, the Neumann boundary condition

$$\boldsymbol{n} \wedge \text{curl}\,\boldsymbol{E}^s = -\boldsymbol{n} \wedge \text{curl}\,\boldsymbol{E}^i \tag{4}$$

should be applied on Γ_{neu}. In the case of a perfect electrical conductor the Dirchlet condition

$$\boldsymbol{n} \wedge \boldsymbol{E}^s = -\boldsymbol{n} \wedge \boldsymbol{E}^i \tag{5}$$

should be applied on Γ_{dir}. When variations in the matearial properties occur, the jump conditions

$$\boldsymbol{n} \wedge (\boldsymbol{E}_a^s - \boldsymbol{E}_b^s) = \boldsymbol{0} \tag{6}$$

$$\boldsymbol{n} \wedge (\mu_a^{-1}\,\text{curl}\boldsymbol{E}_a^s - \mu_b^{-1}\,\text{curl}\boldsymbol{E}_b^s) = -\boldsymbol{n} \wedge (\mu_a^{-1} - \mu_b^{-1})\,\text{curl}\boldsymbol{E}^i \tag{7}$$

should be imposed. In addition, the above boundary and interface conditions should be supplemented by the radiation condition

$$\lim_{r\to\infty} (\boldsymbol{r} \wedge \text{curl}\boldsymbol{E}^s - \mathrm{i}\omega\boldsymbol{E}^s) = 0 \tag{8}$$

to handle the correct behaviour of the field at the infinite extent of the domain Ω.

Combining Maxwell's curl equations for the total fields (1) with those for the incident fields (3), it follows that the scattered electric field satisfies the vector wave equation

$$\text{curl}\mu^{-1}\text{curl}\,\boldsymbol{E}^s - \omega^2\epsilon\boldsymbol{E}^s = \omega^2(\epsilon - I)\boldsymbol{E}^i - \text{curl}\{(\mu^{-1} - I)\text{curl}\,\boldsymbol{E}^i\} \tag{9}$$

where I is the identity tensor. We note that a similar elimination procedure could also be followed for the magnetic field. However, we wish to focus on the solution of the electric field in this report and recover, when required, the magnetic field from equation (1).

With a finite element procedure in mind, we give the weak the variational statement [17]: Find $\boldsymbol{E} \in \boldsymbol{H}_d(\mathrm{curl};\Omega)$ such that

$$(\mu^{-1}\mathrm{curl}\,\boldsymbol{E}^s, \mathrm{curl}\,\boldsymbol{W})_\Omega - \omega^2(\epsilon\boldsymbol{E}^s, \boldsymbol{W})_\Omega = \ell(\boldsymbol{W}) \qquad \forall \boldsymbol{W} \in \boldsymbol{H}_0(\mathrm{curl};\Omega) \tag{10}$$

where $(\cdot,\cdot)_\Omega$ denotes the standard L^2 inner product performed over Ω and ℓ is a linear form defined as

$$\ell(\boldsymbol{W}) = \int_{\Gamma_{neu}} \boldsymbol{W}\cdot\boldsymbol{n}\wedge\mathrm{curl}\,\boldsymbol{E}^i\,\mathrm{d}s + \int_\Omega \omega^2(\epsilon - I)\boldsymbol{E}^i\cdot\boldsymbol{W} - (\mu^{-1} - I)\mathrm{curl}\,\boldsymbol{E}^i\cdot\mathrm{curl}\,\boldsymbol{W}\,\mathrm{d}\Omega \tag{11}$$

The function spaces $\boldsymbol{H}_d(\mathrm{curl};\Omega)$ and $\boldsymbol{H}_0(\mathrm{curl};\Omega)$ introduced above are defined as

$$\boldsymbol{H}_d(\mathrm{curl};\Omega) = \{\boldsymbol{v},\ \boldsymbol{v}\in\boldsymbol{H}(\mathrm{curl};\Omega)\ \boldsymbol{n}\wedge\boldsymbol{v} = -\boldsymbol{n}\wedge\boldsymbol{E}^i,\ \text{on}\ \Gamma_{dir}\}$$

$$\boldsymbol{H}_0(\mathrm{curl};\Omega) = \{\boldsymbol{v},\ \boldsymbol{v}\in\boldsymbol{H}(\mathrm{curl};\Omega)\ \boldsymbol{n}\wedge\boldsymbol{v} = \boldsymbol{0},\ \text{on}\ \Gamma_{dir}\}$$

with

$$\boldsymbol{H}(\mathrm{curl};\Omega) = \{\boldsymbol{v}\in(L^2(\Omega))^2,\ \mathrm{curl}\,\boldsymbol{v}\in L^2(\Omega)\}$$

The end goal is accurately compute the scattering width (or radar cross–section per unit length) distribution. For the two–dimensional problems considered in this report this is defined as

$$\chi(\phi) = \lim_{r\to\infty} 2\pi r\frac{|H_z^s|^2}{|H_z^i|^2} \tag{12}$$

where ϕ is the viewing angle. In particular, we shall consider incident plane waves of the form

$$\boldsymbol{E}^i = \begin{pmatrix} -\sin\theta \\ \cos\theta \end{pmatrix}\exp\{\mathrm{i}\omega(x\cos\theta + y\sin\theta)\} \tag{13}$$

where θ is a specified angle of incidence. For these waves $|H_z^i|^2 = 1$.

3 Approximate weak variational statement

To obtain an approximate weak variational statement, we need to first truncate the infinite domain and approximate the radiation condition (8). This is accomplished by the introduction of an absorbing sponge layer Ω_{pml} which surrounds the truncated free space region Ω_{fs}. It shall be assumed that a single scatterer lies inside the free space region and this may have a dielectric coating Ω_d. For the absorbing sponge layer we shall adopt the perfectly matched layer (PML) approach of Berenger [7] and in particular the curvilinear anisotropic formulation [14, 19]. Inside Ω_{pml} the scattered electric field should satisfy the following non–physical vector wave equation

$$\mathrm{curl}\left(\boldsymbol{\Lambda}^{-1}\mathrm{curl}\,\boldsymbol{E}^s\right) - \omega^2\boldsymbol{\Lambda}\boldsymbol{E}^s = \boldsymbol{0} \tag{14}$$

where $\boldsymbol{\Lambda}$ is a tensor which is constructed so as absorb the outgoing scattered wave [14, 19]. Of course, this can only be done approximately and in general the PML is constructed so as to perfectly absorb outgoing waves propagating at a certain angle, for all other directions, the absorption is approximate. Nevertheless very accurate results can be accomplished with the PML approach. The boundary condition $\boldsymbol{n}\wedge\boldsymbol{E}^s = \boldsymbol{0}$ at the exterior boundary Γ_{far} of Ω_{pml} completes the approximation to the radiation condition. The complete arrangement of the scattering problem is illustrated in Figure 1.

Corresponding to the PML formulation, we introduce the solution and weighting spaces as

$$X_d = \{\boldsymbol{v}, \boldsymbol{v}\in\boldsymbol{H}(\mathrm{curl};\Omega), \boldsymbol{n}\wedge\boldsymbol{v} = -\boldsymbol{n}\wedge\boldsymbol{E}^i\ \text{on}\ \Gamma_{dir}\ , \boldsymbol{n}\wedge\boldsymbol{v} = \boldsymbol{0}\ \text{on}\ \Gamma_{far}\}$$

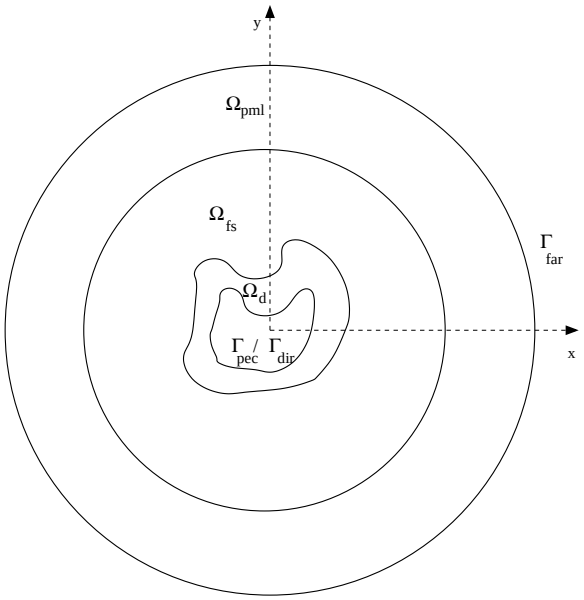

Figure 1: The arrangement of the electromagnetic scattering problem.

and

$$X_0 = \{\boldsymbol{v}, \boldsymbol{v} \in \boldsymbol{H}(\text{curl}; \Omega), \boldsymbol{n} \wedge \boldsymbol{v} = \boldsymbol{0} \text{ on } \Gamma_{dir} \ , \boldsymbol{n} \wedge \boldsymbol{v} = \boldsymbol{0} \text{ on } \Gamma_{far}\}$$

The approximate weak variational statement to the problem is then: find $\boldsymbol{E}^s \in X_d$ such that

$$(\mu^{-1}\text{curl}\, \boldsymbol{E}^s, \text{curl}\, \boldsymbol{W})_{\Omega_{fs}+\Omega_d+\Omega_{pml}} - \omega^2(\epsilon \boldsymbol{E}^s, \boldsymbol{W})_{\Omega_{fs}+\Omega_d+\Omega_{pml}} = \ell(\boldsymbol{W})_{\Omega_d} \qquad \forall \boldsymbol{W} \in X_0 \qquad (15)$$

where we set $\epsilon = \mu = \boldsymbol{\Lambda}$ inside Ω_{pml} and $\epsilon = \mu = I$ inside Ω_{fs}. Note the modified definition of the linear form

$$\ell(\boldsymbol{W})_{\Omega_d} = \int_{\Gamma_{neu}} \boldsymbol{W} \cdot \boldsymbol{n} \wedge \text{curl}\, \boldsymbol{E}^i \ \text{d}s + \int_{\Omega_d} \omega^2(\epsilon - I)\boldsymbol{E}^i \cdot \boldsymbol{W} - (\mu^{-1} - I)\text{curl}\, \boldsymbol{E}^i \cdot \text{curl}\, \boldsymbol{W}\, \text{d}\Omega \quad (16)$$

which is to account for the un–physical PML layer.

Following a Galerkin finite element procedure, we replace the continuous spaces with discrete subspaces $X_d^H \subset X_d$ and $X_0^H \subset X_0$ and solve for discrete solutions $\boldsymbol{E}_H^s \in X_d^H$. The discrete weak variational statement is then: Find $\boldsymbol{E}_H^s \in X_d^H$ such that

$$(\mu^{-1}\text{curl}\, \boldsymbol{E}_H^s, \text{curl}\, \boldsymbol{W}_H)_{\Omega_{fs}+\Omega_d+\Omega_{pml}} - \omega^2(\epsilon \boldsymbol{E}_H^s, \boldsymbol{W}_H)_{\Omega_{fs}+\Omega_d+\Omega_{pml}} = \ell(\boldsymbol{W}_H)_{\Omega_d} \qquad \forall \boldsymbol{W}_H \in X_0^H \qquad (17)$$

In the next section we shall discuss the discretisation which leads to an approximate solution of this equation.

4 Plane wave $\boldsymbol{H}$(curl) conforming discretisation

We follow our previous work [20] and introduce the plane wave $\boldsymbol{H}$(curl) conforming basis functions for quadrilateral and triangular elements.

4.1 Quadrilateral element

The lowest order ($p = 0$) $\boldsymbol{H}$(curl) conforming basis functions for quadrilateral elements may be expressed, over the reference square element $-1 \leq \xi, \eta \leq 1$ shown in Figure 2, as

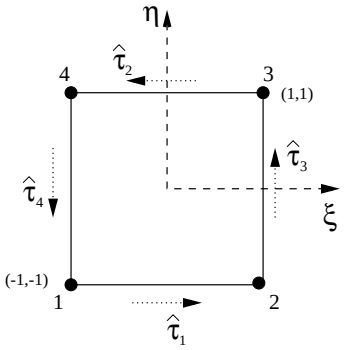

Figure 2: Reference quadrilateral element.

$$\hat{\boldsymbol{\phi}}_1^q = \frac{1}{2}(1-\eta)\begin{pmatrix} 1 \\ 0 \end{pmatrix} \qquad \hat{\boldsymbol{\phi}}_2^q = \frac{1}{2}(1+\eta)\begin{pmatrix} -1 \\ 0 \end{pmatrix} \tag{18}$$

$$\hat{\boldsymbol{\phi}}_3^q = \frac{1}{2}(1+\xi)\begin{pmatrix} 0 \\ 1 \end{pmatrix} \qquad \hat{\boldsymbol{\phi}}_4^q = \frac{1}{2}(1-\xi)\begin{pmatrix} 0 \\ -1 \end{pmatrix} \tag{19}$$

where the presence of the hat denotes a vector expressed relative to the reference coordinate system (ξ, η). In the usual manner, the variation of the solution over the element is expressed in the form

$$\hat{\boldsymbol{E}}_H = \begin{pmatrix} \hat{E}_{H\xi} \\ \hat{E}_{H\eta} \end{pmatrix} = \sum_{i=1}^{4} e_i \hat{\boldsymbol{\phi}}_i^q \tag{20}$$

The degrees of freedom for the lowest order edge element are defined as

$$\boldsymbol{E}_H \rightarrow \int_{\gamma_i} L_0 \boldsymbol{\tau}_i \cdot \boldsymbol{E}_H \mathrm{d}\gamma \tag{21}$$

where γ_i and $\boldsymbol{\tau}_i$ are the parameterization and tangent vector in the (x, y) coordinate system to the i'th edge, respectively. $L_0 = 1$ is the zero'th order Legendre polynomial. It follows that the unknown scalar coefficients, e_i, satisfy the relations

$$e_i = \boldsymbol{\tau}_i \cdot \boldsymbol{E}_H|_i \qquad i = 1, 2, 3, 4 \tag{22}$$

due to the fact that on an edge i, $\hat{\boldsymbol{\tau}}_i \cdot \hat{\boldsymbol{\phi}}_j^q|_i = 0$ for $i \neq j$ and $\hat{\boldsymbol{\tau}}_i \cdot \hat{\boldsymbol{\phi}}_j^q|_i = 1$ for $i = j$. This results in a scheme with a constant tangential component of the field along the edges of the element. In the plane wave basis approach, we choose to represent e_i as an expansion of M plane waves [16, 15]

$$e_i = \sum_{m=1}^{M(i)} A_i^m \exp\{\mathrm{i}\omega(x\cos\theta_m + y\sin\theta_m)\} \tag{23}$$

where A_i^m are unknown complex valued coefficients and θ_m are the plane wave directions. In general, the number of directions $M(i)$ may vary on different edges. For this approach, the degrees of freedom are defined as

$$\boldsymbol{E}_H \rightarrow \int_{\gamma_i} \exp\{\mathrm{i}\omega(x\cos\theta_n + y\sin\theta_n)\}\boldsymbol{\tau}_i \cdot \boldsymbol{E}_H \mathrm{d}\Gamma \qquad n = 1, \cdots, M(i) \tag{24}$$

The approximation $\hat{\boldsymbol{E}}_H$ is then given by

$$\hat{\boldsymbol{E}}_H = \sum_{i=1}^{4} \hat{\boldsymbol{\phi}}_i^q \sum_{m=1}^{M(i)} A_i^m \exp\{\mathrm{i}\omega(x\cos\theta_m + y\sin\theta_m)\} \tag{25}$$

or as

$$\hat{\boldsymbol{E}}_H = \sum_{i=1}^{4} \sum_{m=1}^{M(i)} A_i^m \hat{\boldsymbol{\psi}}_i^m \tag{26}$$

where $\hat{\boldsymbol{\psi}}_i^m$ are new vector shape functions which are defined as

$$\hat{\boldsymbol{\psi}}_i^m = \hat{\boldsymbol{\phi}}_i^q \exp\{\mathrm{i}\omega(x\cos\theta_m + y\sin\theta_m)\} \tag{27}$$

We will need to determine the components of $\hat{\boldsymbol{E}}_H$ in the (x, y) coordinate system, but, we postpone the details of how this may be accomplished until after the presentation of the basis functions for the triangular element.

4.2 Triangular element

The lowest order $\boldsymbol{H}$(curl) conforming basis functions for triangular elements may be expressed, over the equilateral triangular reference element shown in Figure 3, in the form

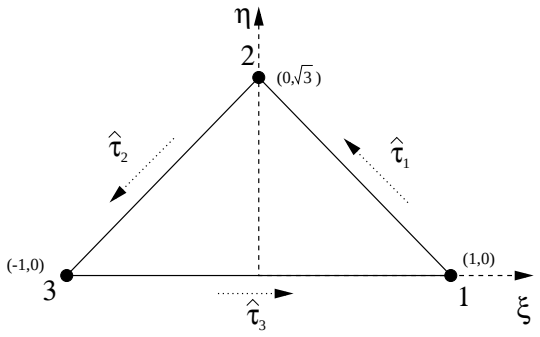

Figure 3: Reference triangular element.

$$\hat{\boldsymbol{\phi}}_1^t = 2(\lambda_1 \mathrm{grad}\,\lambda_2 - \lambda_2 \mathrm{grad}\,\lambda_1) \qquad \hat{\boldsymbol{\phi}}_2^t = 2(\lambda_2 \mathrm{grad}\,\lambda_3 - \lambda_3 \mathrm{grad}\,\lambda_2) \tag{28}$$

$$\hat{\boldsymbol{\phi}}_3^t = 2(\lambda_3 \mathrm{grad}\,\lambda_1 - \lambda_1 \mathrm{grad}\,\lambda_3) \tag{29}$$

and the approximation of the solution over the element written as

$$\hat{\boldsymbol{E}}_H = \sum_{i=1}^{3} e_i \hat{\boldsymbol{\phi}}_i^t \tag{30}$$

Here the symbols $\lambda_1, \lambda_2, \lambda_3$ denote the area coordinates of the master triangle and these can be defined as

$$\lambda_1 = \frac{1}{2\sqrt{3}}(\sqrt{3} + \sqrt{3}\xi - \eta) \qquad \lambda_2 = \frac{1}{\sqrt{3}}\eta \tag{31}$$

$$\lambda_3 = \frac{1}{2\sqrt{3}}(\sqrt{3} - \sqrt{3}\xi - \eta) \tag{32}$$

These area coordinates satisfy the condition $\lambda_i(\xi_j, \eta_j) = \delta_{ij}$, where (ξ_j, η_j) are the coordinates of vertex j and δ_{ij} is the Kronecker delta.

The triangular element basis functions given in equations (28) and (29) satisfy $\hat{\boldsymbol{\tau}}_i \cdot \hat{\boldsymbol{\phi}}_j^t|_i = 0$ on an edge i for $i \neq j$ and $\hat{\boldsymbol{\tau}}_i \cdot \hat{\boldsymbol{\phi}}_j^t|_i = 1$ for $i = j$. In a similar manner to the quadrilateral basis, we choose to represent e_i as an expansion of plane waves such that

$$\hat{\boldsymbol{E}}_H = \sum_{i=1}^{3} \hat{\boldsymbol{\phi}}_i^t \sum_{m=1}^{M(i)} A_i^m \exp\{\mathrm{i}\omega(x\cos\theta_m + y\sin\theta_m)\} \tag{33}$$

or, equivalently, as

$$\hat{\boldsymbol{E}}_H = \sum_{i=1}^{3} \sum_{m=1}^{M(i)} A_i^m \hat{\boldsymbol{\psi}}_i^m \tag{34}$$

where

$$\hat{\boldsymbol{\psi}}_i^m = \hat{\boldsymbol{\phi}}_i^t \exp\{\mathrm{i}\omega(x\cos\theta_m + y\sin\theta_m)\} \tag{35}$$

are the new vector shape functions.

4.3 Covariant mapping

We will be interested in determining the components of a vector shape function $\hat{\boldsymbol{\psi}}$ in the (x, y) coordinate system. If the components of $\hat{\boldsymbol{\psi}}$ in the reference coordinate system are $\hat{\boldsymbol{\psi}} = (\hat{\psi}_\xi, \hat{\psi}_\eta)^T$, and we write $\boldsymbol{\psi} = (\psi_x, \psi_y)^T$ for the vector shape function expressed in the (x, y) coordinate system, it follows from a covariant mapping [30] that

$$\boldsymbol{\psi} = \boldsymbol{J}^{-T} \begin{pmatrix} \hat{\psi}_\xi \\ \hat{\psi}_\eta \end{pmatrix} \tag{36}$$

where J is the Jacobian matrix, which is defined as

$$\boldsymbol{J} = \begin{pmatrix} \dfrac{\partial x}{\partial \xi} & \dfrac{\partial x}{\partial \eta} \\ \dfrac{\partial y}{\partial \xi} & \dfrac{\partial y}{\partial \eta} \end{pmatrix} \tag{37}$$

If a linear representation of the geometry is adopted, the standard bilinear shape functions

$$N_1 = \frac{1}{4}(1-\xi)(1-\eta) \qquad N_2 = \frac{1}{4}(1+\xi)(1-\eta) \tag{38}$$

$$N_3 = \frac{1}{4}(1+\xi)(1+\eta) \qquad N_4 = \frac{1}{4}(1-\xi)(1+\eta) \tag{39}$$

can be employed to construct a mapping from (ξ, η) to (x, y) for the quadrilateral element. Explicitly, this mapping is given by

$$\begin{pmatrix} x \\ y \end{pmatrix} = \sum_{i=1}^{4} N_i \begin{pmatrix} x_i \\ y_i \end{pmatrix} \tag{40}$$

where (x_i, y_i) $i = 1, 2, 3, 4$ are the nodal coordinates. For the triangular element the corresponding mapping is

$$\begin{pmatrix} x \\ y \end{pmatrix} = \sum_{i=1}^{3} \hat{\lambda}_i \begin{pmatrix} x_i \\ y_i \end{pmatrix} \tag{41}$$

where $\hat{\lambda}_i$ are the area coordinates defined in equations (31) and (32). When curved geometries are required we use a blending function approach [32] to give an exact boundary resolution. The expression

$$\operatorname{curl} \boldsymbol{\psi} = \frac{1}{|\boldsymbol{J}|} \left(\frac{\partial \hat{\psi}_\eta}{\partial \xi} - \frac{\partial \hat{\psi}_\xi}{\partial \eta} \right) \tag{42}$$

is used to evaluate $\operatorname{curl} \boldsymbol{\psi}$ in terms of the reference coordinate system. The differentiation required for this expression is achieved through repeated use of the chain rule.

5 Computational procedure

Following discretisation of equation (17) by the plane wave $\boldsymbol{H}$(curl) conforming basis one obtains the linear equation system

$$\boldsymbol{B}\boldsymbol{u} = \boldsymbol{r} \tag{43}$$

with typical entries

$$B_{ij} = \int_{\Omega_{fs}+\Omega_d+\Omega_{pml}} \mu^{-1}\mathrm{curl}\,\boldsymbol{\psi}_i \cdot \mathrm{curl}\,\boldsymbol{\psi}_j - \omega^2\epsilon\boldsymbol{\psi}_i \cdot \boldsymbol{\psi}_j \mathrm{d}\Omega \tag{44}$$

$$r_i = \int_{\Gamma_{neu}} \boldsymbol{\psi}_i \cdot \boldsymbol{n} \wedge \mathrm{curl}\boldsymbol{E}^i \mathrm{d}s + \int_{\Omega_d} \omega^2(\epsilon - I)\boldsymbol{E}^i \cdot \boldsymbol{\psi}_i - (\mu^{-1} - I)\mathrm{curl}\,\boldsymbol{E}^i \cdot \mathrm{curl}\,\boldsymbol{\psi}_i \mathrm{d}\Omega \tag{45}$$

Note that when a Cuthill–Mckee re-numbering of the edges is performed and the unknowns are carefully numbered this system becomes banded in nature. In this section we shall comment on how the plane wave directions may be chosen and how the evaluation of the integrals may be accomplished. We shall also propose a new method which uses our plane wave basis to obtain an accurate computation of the scattering width output.

5.1 Selection of the plane wave directions

We first describe how the plane wave directions may be selected for Dirchlet boundary conditions. Next we describe how the directions inside the mesh may be chosen in such a way so as to control the condition number of the global matrix.

5.1.1 Dirchlet boundary conditions

First let us observe that the boundary condition $\boldsymbol{n}\wedge\boldsymbol{E}^s = -\boldsymbol{n}\wedge\boldsymbol{E}^i$ may be equivalently written as $\boldsymbol{\tau}\cdot\boldsymbol{E}^s = -\boldsymbol{\tau}\cdot\boldsymbol{E}^i$ in two–dimensions. One might wish to determine the coefficients A_i^m corresponding to the known coefficients for an edge i aligned with a Dirchlet boundary by solving an L^2 minimisation problem.

$$(\boldsymbol{\tau}\cdot\boldsymbol{E}_H, \boldsymbol{\tau}\cdot\boldsymbol{\psi}_i^m)_\Gamma = -(\boldsymbol{\tau}\cdot\boldsymbol{E}^i, \boldsymbol{\tau}\cdot\boldsymbol{\psi}_i^m)_\Gamma \qquad m = 1, \cdots M(i) \tag{46}$$

where $(,)_\Gamma$ is an L^2 inner product on an edge of Γ. However, when linear geometry is considered, and one of the plane wave directions is selected to be the same as the incident wave, it follows that only the coefficient corresponding to the incident direction is non–zero. Thus the solution to this often ill–conditioned system can be avoided.

To show that this is the case, we now consider an example consisting of a single Dirchlet edge with $M = 4$ plane wave directions. We obtain the linear system

$$C^2\int_\gamma \begin{pmatrix} b_1^2 & b_1b_2 & b_1b_3 & b_1b_4 \\ b_2b_1 & b_2^2 & b_2b_3 & b_2b_4 \\ b_3b_1 & b_3b_2 & b_3^2 & b_3b_4 \\ b_4b_1 & b_4b_2 & b_4b_3 & b_4^2 \end{pmatrix} \mathrm{d}\Gamma \begin{pmatrix} A_i^1 \\ A_i^2 \\ A_i^3 \\ A_i^4 \end{pmatrix} = C(\tau_x\sin\theta - \tau_y\cos\theta)\int_\gamma \begin{pmatrix} b_1d \\ b_2d \\ b_3d \\ b_4d \end{pmatrix} \mathrm{d}\Gamma \tag{47}$$

where the entries are of the form

$$b_i = \exp\{\mathrm{i}\omega(x\cos\theta_i + y\sin\theta_i)\} \qquad d = \exp\{\mathrm{i}\omega(x\cos\theta + y\sin\theta)\} \tag{48}$$

and the constant $C = \tau_x\phi_{ix} + \tau_y\phi_{iy}$ which arises from the tangential component of the standard lowest order basis function may be taken outside the integral. If we select $\theta_1 = \theta$ and $\theta_2 \neq \theta_3 \neq \theta_4 \neq \theta$ then we arrive at the solution

$$A_i^1 = \frac{\tau_x\sin\theta - \tau_y\cos\theta}{C} \qquad A_i^2 = A_i^3 = A_i^4 = 0 \tag{49}$$

A complication arises in the case of curved elements as $\tau_x \sin\theta - \tau_y \cos\theta$ is no longer a constant. For curved elements, we propose the following approximation to the Dirchlet boundary condition which avoids the computation of the solution to the ill conditioned linear system

$$A_i^1 = \frac{\tau_x|_{\overline{\gamma}} \sin\theta - \tau_y|_{\overline{\gamma}} \cos\theta}{C} \qquad A_i^2 = A_i^3 = A_i^4 = 0 \tag{50}$$

in the above $\boldsymbol{\tau}|_{\overline{\gamma}} = (\tau_x|_{\overline{\gamma}}, \tau_y|_{\overline{\gamma}})^T$ is the tangent vector evaluated at the midpoint of the edge (the constant C is un–affected by the curved geometry). Note that in the case of Neumann boundary conditions, no special selection of the directions is required as one may directly evaluate the contribution to the right hand side vector (45).

5.1.2 Interior edges

In our previous experiments with the plane wave basis, it was found that the condition number of the global matrix grows rapidly as the number of directions is increased [20]. Therefore, we propose to select the number and directions of the plane waves on interior edges in the mesh in such a way that the condition number of the global matrix is controlled. What we propose is a similar approach to that which Monk *et. al.* employed to select the directions of the waves in their ultra weak formulation [24]. In our approach, the assessment is based on the computation of the condition number

$$\kappa(\boldsymbol{B}^e) = \|\boldsymbol{B}^e\|_2 \cdot \|(\boldsymbol{B}^e)^{-1}\|_2 = \frac{\max s_i(\boldsymbol{B}^e)}{\min s_i(\boldsymbol{B}^e)} \tag{51}$$

of elemental matrices $\boldsymbol{B}^e$ where s_i are the singular values. The matrix $\boldsymbol{B}^e$ has typical entries

$$B_{ij}^e = \int_{\Omega_e} \mu^{-1} \mathrm{curl}\, \boldsymbol{\psi}_i \cdot \mathrm{curl}\, \boldsymbol{\psi}_j - \omega^2 \epsilon \boldsymbol{\psi}_i \cdot \boldsymbol{\psi}_j \mathrm{d}\Omega \tag{52}$$

where Ω^e is the elemental area. To compute the allowable directions, the following procedure is performed

1. Set κ_{max} to be the maximum allowable condition number and M_{max} to be the maximum number of allowable directions.
2. For i=1,nelem{
   (a) Set $M = M_{max}$ for all edges of the element;
   (b) Select the directions of the plane waves on each edge of the element as $\theta_j = 2\pi j/M$ with $j = 1, \cdots, M$;
   (c) Compute $\kappa(\boldsymbol{B}^e)$;
   (d) If $\kappa(\boldsymbol{B}^e) > \kappa_{max}$ { Set $M = M - 1$; goto b}}
3. For i=1,ne{
   (a) Compare the number of directions on an edge i for neighbouring elements M_l and M_r and set $M(i) = \min(M_l, M_r)$}

In the above nelem is the number of elements and ne is the number of interior edges in the mesh. The above procedure make use of the result that $\kappa(\boldsymbol{B}^e) \geq \kappa(\boldsymbol{A})$. If κ_{max} is not exceeded, all edges are enriched with M_{max} plane wave directions. Currently the directions are selected to be uniformly spaced, however it is acknowledged that this may not be the best choice. A better selection may perhaps be obtained by using ray techniques to determine the directions of the plane waves.

5.2 Evaluation of integrals

Due to the presence of the PML and the use of blending functions for the curved boundaries, the integrals are non standard and therefore high–degree Gauss quadrature rules are used to evaluate the expressions. However, special analytical integration along the lines suggested by Bettess *et. al.* [9] could possibly be developed which would improve the efficiency of the approach.

5.3 Evaluation of the scattering width

Following a near to far field transformation, the scattering width may be evaluated from the functional [17]

$$\chi_H(\phi) = \frac{\omega}{4}\left|\int_{\Gamma_c} \boldsymbol{n}\wedge\boldsymbol{E}_H^s\cdot\boldsymbol{V} + \boldsymbol{n}\wedge\operatorname{curl}\boldsymbol{E}_H^s\cdot\boldsymbol{Y}\,\mathrm{d}\Gamma'\right|^2 \tag{53}$$

where Γ_c is a collection surface, which is chosen to completely surround the scatterer. The value of the scattering width, measured in decibels, is given by $10\log(\chi(\phi))$. The vectors $\boldsymbol{V}$ and $\boldsymbol{Y}$ are functions of the viewing angle ϕ and are defined as

$$\boldsymbol{V} = \begin{pmatrix} 0 \\ 0 \\ -1 \end{pmatrix} \exp\{\mathrm{i}\omega(x'\cos\phi + y'\sin\phi)\} \tag{54}$$

$$\boldsymbol{Y} = \frac{1}{\mathrm{i}\omega}\begin{pmatrix} \sin\phi \\ -\cos\phi \\ 0 \end{pmatrix} \exp\{\mathrm{i}\omega(x'\cos\phi + y'\sin\phi)\} \tag{55}$$

A basic approach to computing the scattering width is obtained by directly evaluating (53). However in this approach the flux term $\boldsymbol{n}\wedge\operatorname{curl}\boldsymbol{E}_H^s$ is not calculated carefully, and accuracy may be lost in the computation of the scattering width. To this end, as a more sophisticated approach, we employ the technique proposed by Monk [25, 23], who suggests using the variational statement to approximate the flux term. In this case, it is convenient to rewrite the scattering width as [17, 21]

$$\chi_H(\phi) = \frac{\omega}{4}\mathcal{L}^o(\boldsymbol{E}_H;\phi)\overline{\mathcal{L}^o(\boldsymbol{E}_H;\phi)} \tag{56}$$

where the functional $\mathcal{L}^o(\boldsymbol{E}_H;\phi)$ is defined as

$$\mathcal{L}^o(\boldsymbol{E}_H;\phi) = \int_{\Gamma_c} \boldsymbol{n}\wedge\boldsymbol{E}_H\cdot\boldsymbol{V}\,\mathrm{d}\Gamma + \sum\int_k \left(\omega^2\boldsymbol{E}_H\cdot\boldsymbol{Y}_H - \operatorname{curl}\boldsymbol{E}_H\cdot\operatorname{curl}\boldsymbol{Y}_H\right)\mathrm{d}\Omega' \tag{57}$$

Here, the summation extends over all elements $k\in\Omega$ such that $\partial k\cup\Gamma_c\neq\emptyset$ and $\boldsymbol{Y}_H$ is the plane wave $\boldsymbol{H}$(curl) interplant of $\boldsymbol{Y}$. We can determine the coefficients of $\boldsymbol{Y}_H$ by following a similar procedure to that which was already described for determining the coefficients for the Dirchlet boundary conditions.

6 Numerical experiments

In this section we present a selection of numerical experiments to demonstrate the performance of our proposed procedure. All the examples presented will be measured in terms of the size of the electrical length. This is a representative dimension of the object (eg diameter of a cylinder) measured in terms of incident wave lengths. The higher the electrical length, the more complex the problem. In particular, we shall apply the approach to scattering by circular PEC and PMC cylinders which have exact analytical solutions and asses the accuracy of the original and improved methods for calculation of the scattering width. We will also undertake comparisons of the computational efficiency of the plane wave approach with that of a *hp* version approach [17, 19, 21]. This is a challenging comparison as the *hp* approach has already been observed to be very competitive for scattering problems.

Furthermore we shall present numerical examples with dielectric coatings in which the material properties take non–identity values. For these examples we shall consider PEC and PMC cylinders with a thin dielectric coatings and use analytical solutions to asses the accuracy of the approach. Finally, we will asses the predictive capability of the approach by applying it to non–circular scatterers which have no analytical solution. We asses the accuracy of the proposed procedure for these problems by undertaking comparisons with the *hp* version finite element code.

6.1 Perfectly conducting cylinders

Initially we consider scattering of a plane wave by circular cylinders with PEC and PMC boundaries and electrical length 2λ. For these examples we consider waves with an angle of propagation $\theta = 0$. We consider a mesh of quadrilateral elements in the form of a circular annulus with inner radius $r = 1$ and outer radius $r = 2$. The spacing is chosen as 3 points per wavelength and the blending function approach is used to represent the geometry. An illustration of the mesh, without the blending function correction, is shown in Figure 4 (a). We select $M_{max} = 8$, and for this choice the corresponding scattering width distributions are shown in Figure 4 (b) and (c). In this figure scattering width distributions corresponding to the analytical solutions are also shown. For each scatterer, the plane wave scattering width distributions are computed using two different approaches: the basic approach and the more sophisticated approach described in Section 5.3. When the sophisticated method for calculating the scattering width distribution is adopted, very accurate results are obtained. The more naive approach leads to an inaccurate solution.

We note that for meshes with spacings coarser than 3 points per wavelength inaccurate scattering width distributions are obtained with the plane wave approach, even if the more sophisticated method is used. This is due to the approximations inherent in the underlying $p = 0$ basis functions and the approximations introduced in the application of Dirchlet boundary conditions on curved meshes. These problems could be addressed by increasing the order of the underlying $\boldsymbol{H}(\text{curl})$ conforming approximation. But this is beyond the scope of this report.

As a second example we consider scattering by circular cylinders of electrical length 8λ with PEC and PMC boundaries. Again we employ a mesh of quadrilaterial elements in the form of a circular annulus with inner radius $r = 1$ and outer radius $r = 2$. The mesh spacing of 3 points per wave length is retained and the blending function approach is used to represent the geometry. An illustration of the mesh without the blending function correction is shown in Figure 5 (a). As it is already apparent that the more sophisticated scattering width computation performs substantially better than the basic approach, we shall henceforth only show results for the sophisticated approach. In Figure 5 (b) and (c) we show the computed scattering width distributions obtained with $M_{max} = 8$ directions. In this figure we observe that a very accurate prediction of the scattering width is obtained for both PEC and PMC scatterers. Note that if the PML is coupled with an absorbing boundary condition it is expected that these accurate results could be maintained even if Γ_{far} is placed very close to the object [17].

Next, we compare the performance of the plane wave approach with that of the *hp* version approach. We undertake computations for the 2λ and 8λ PEC and PMC cylinders and employ the same meshes that were previously described. In Figure 6 we present the scattering width distributions obtained in the 2λ case. We observe that a comparable accuracy for both PEC and PMC cylinders is obtained when uniform $p = 3$ elements are employed. In Table 1 we present a comparison of the computational resources that are required by the two approaches. We observe that the total number unknowns used in the plane wave approach is about half that for the *hp*–version approach. However, the size of the linear system that should be solved in the case of the *hp* approach is smaller than that for the plane wave approach. This is because in the *hp*–version approach the interior degrees of freedom (which for high p make up the majority) can be eliminated through static condensation [17].

In Figure 7 we present findings for the cylinders of electrical length 8λ. We obtain comparable accuracy to the plane wave approach for both PEC and PMC cylinders when uniform $p = 3$ elements are employed. In Table 2 we present a comparison of the computational resources that are required for the two approaches. As in the 2λ case, we observe that the total number of unknowns for the plane wave approach is about half that for the *hp* version approach. Although, in the *hp* approach the size of the linear system is smaller.

In order to make a fair comparison to the *hp* version approach, we should note that only the plane wave approach is limited by the 3 points per wavelength restriction. For the *hp*–version approach one could adopt coarser mesh spacings than those presented here and still obtain accurate results, as shown in [17]. For coarser meshes, a smaller numbers of unknowns would be required, albeit at the computational cost of a slightly larger linear system. Reductions in the number of unknowns required for the plane wave approach could also be obtained if the a more sophisticated

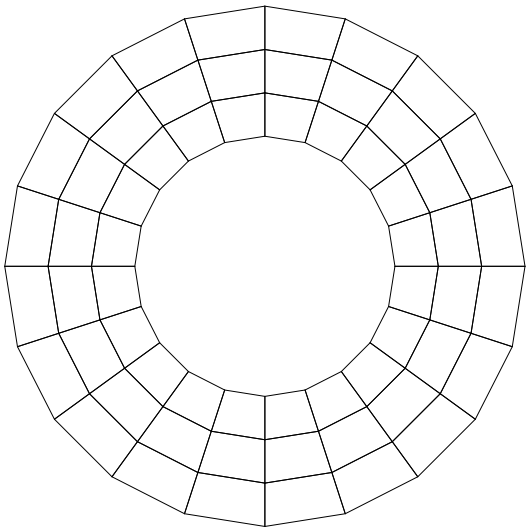

(a)

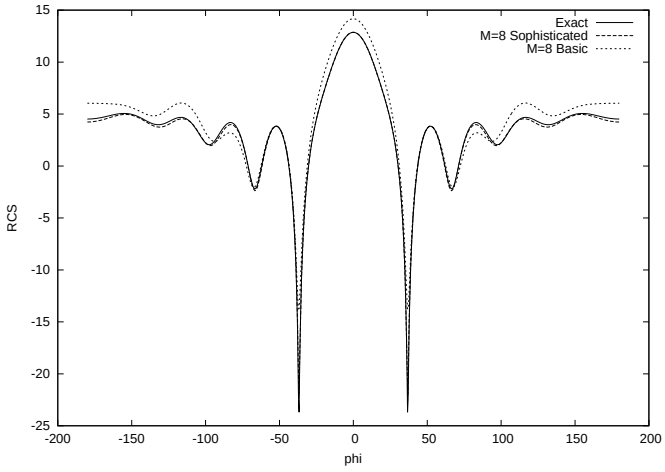

(b)

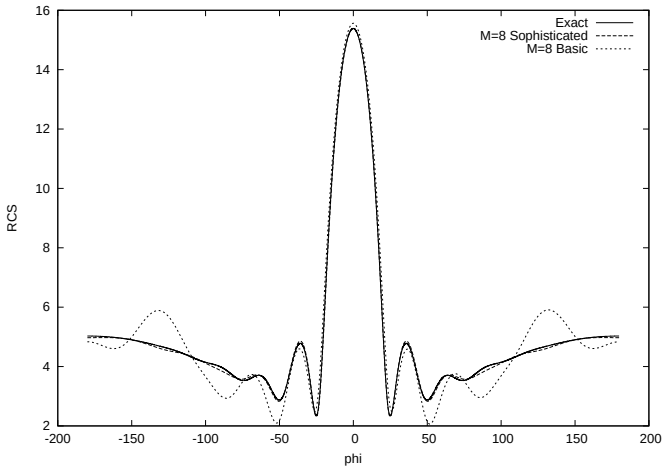

(c)

Figure 4: Scattering by a cylinder of electrical length 2λ showing: (a) a mesh with 3pts/λ, (b) PEC scattering width distribution and (c) PMC scattering width distribution.

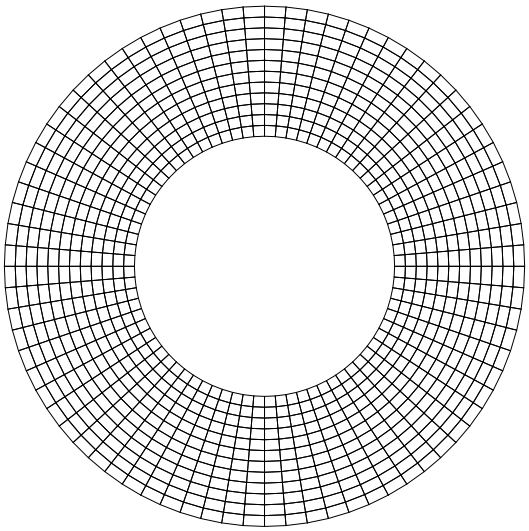

(a)

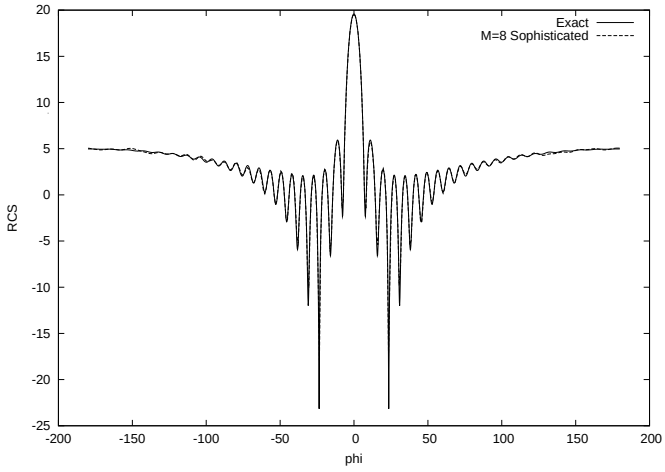

(b)

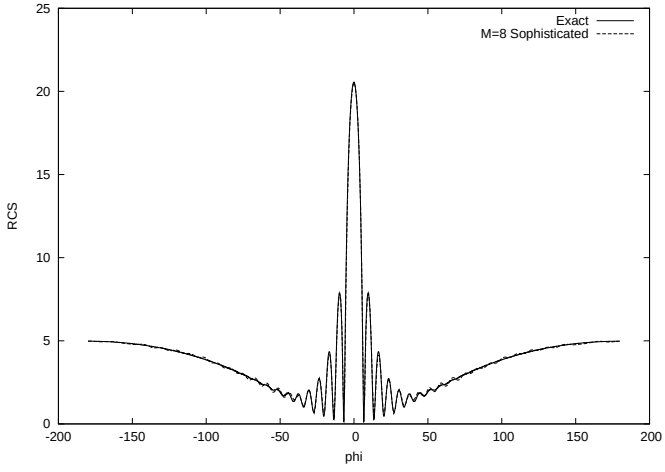

(c)

Figure 5: Scattering by a cylinder of electrical length 8λ showing: (a) a mesh with 3pts/λ, (b) PEC scattering width distribution and (c) PMC scattering width distribution.

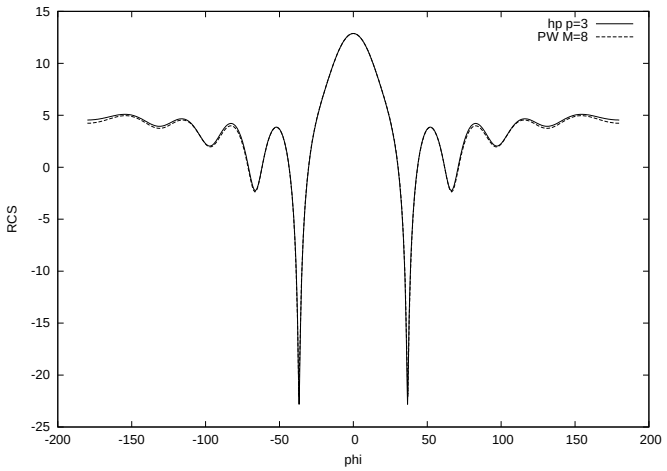

(a)

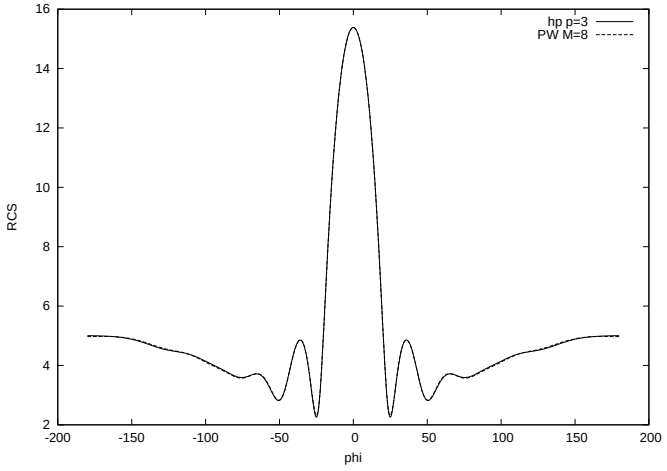

(b)

Figure 6: Scattering by a cylinder of electrical length 2λ showing comparisons of the scattering width distribution for the PW version and *hp*–version in the cases of: (a) a PEC cylinder and (b) a PMC cylinder.

	Total Unknowns	Linear Solver Dimension	Bandwidth
hp–version PEC	1920	480	116
PW version PEC	900	900	232
hp–version PMC	2000	560	116
PW version PMC	1080	1080	232

Table 1: Comparison of the number of unknowns required by the PW version and *hp*–version $\boldsymbol{H}$(curl) conforming finite element methods in order to obtain comparable accuracy for a 2λ cylinder.

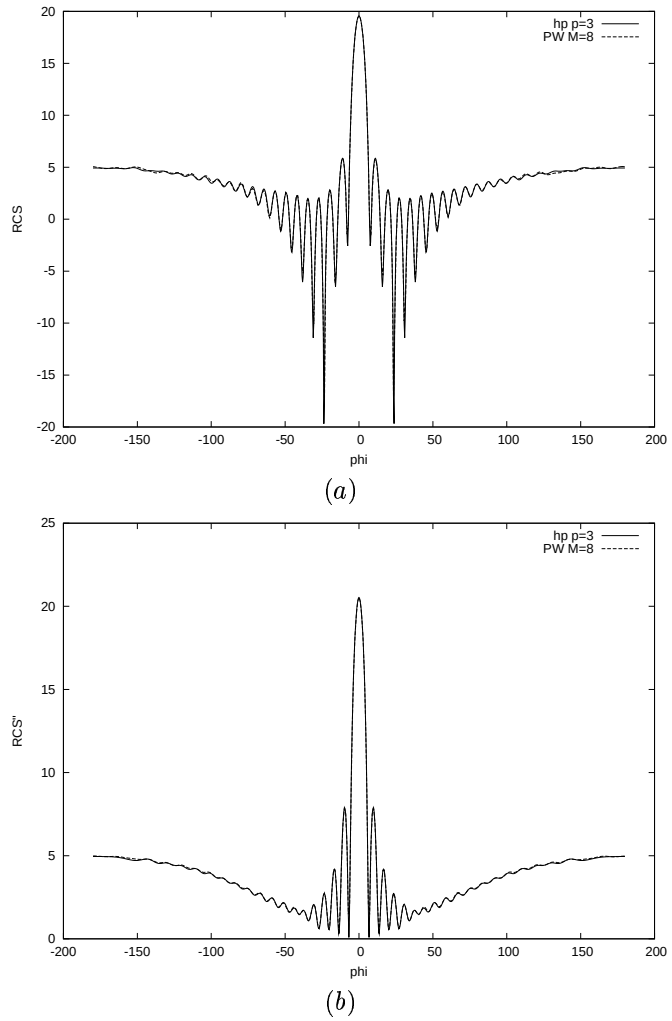

Figure 7: Scattering by a cylinder of electrical length 8λ showing comparisons of the scattering width distribution for the PW version and *hp*–version in the cases of: (*a*) a PEC cylinder and (*b*) a PMC cylinder.

	Total Unknowns	Linear Solver Dimension	Bandwidth
hp–version PEC	29488	7600	404
PW version PEC	16412	16412	808
hp–version PMC	29184	7296	404
PW version PMC	15804	15804	808

Table 2: Comparison of the number of unknowns required by the PW version and *hp*–version $\boldsymbol{H}(\mathrm{curl})$ conforming finite element methods in order to obtain comparable accuracy for a 8λ cylinder.

method was adopted for choosing the directions.

6.2 Coated perfectly conducting cylinders

In this section we explore the application of the plane wave approach to cylinders with a dielectric coating. We consider cylinders of electrical length 8λ with coatings of thickness $2\lambda/3$. The material properties of the coating are

$$\epsilon = 2.56 \qquad \mu = 1 \tag{58}$$

For this example we use a hybrid mesh of quadrilaterals and triangles with mesh spacing 3 points per wavelength. An illustration of the mesh is shown in Figure 8 (a). The dielectric region is composed of the first 2 layers of triangular elements. In Figure 8 (b) and (c) the scattering width distributions for PEC and PMC coated cylinders are presented. In these plots we show the distributions obtained when plane wave elements with $M_{max} = 8$ directions are used alongside those distributions obtained with a hp–version approach using uniform $p = 4$ elements. For both the PEC and PMC cylinders, excellent agreement with the analytical solutions are obtained with the plane wave and the hp approaches.

	Total Unknowns	Linear Solver Dimension	Bandwidth
hp–version PEC	42990	9990	565
PW version PEC	17316	17316	904
hp–version PMC	43360	10360	565
PW version PMC	17390	17390	904

Table 3: Comparison of the number of unknowns required by the PW version and hp–version $\boldsymbol{H}$(curl) conforming finite element methods in order to obtain comparable accuracy for a coated 8λ cylinder.

It is perhaps quite suprising that the plane wave conforming elements perform so well for the coated perfectly conducting cylinders, especially as the exponential functions contained in the basis functions contain the free space frequency and not the wavenumber in the dielectric medium. Nevertheless the results produced clearly demonstrate that using plane wave basis functions, originally designed for free space regions, do not encounter difficulties when applied to problems with dielectric materials. In the Appendix A the use of planewave approach for dielectric matearials is discussed in more detail.

In Table 3 we give a comparison of the computational resources required for the hp and plane wave approaches. As in the previous perfectly conducting examples, the total number of unknowns required in the plane wave approach is about half that in the hp version approach. The size of the linear system to be solved in the hp approach is smaller than that in the plane wave approach.

6.3 Non–cylindrical cavities

In this final section, we apply the plane wave approach to a selection of non–cylindrical cavities. First we consider scattering by a 4λ PEC U shaped cavity rotated through 90 degrees. The thickness of the walls are denoted by d and the outer dimensions are given by $b+d$ in the x direction and $c + 2d$ in the y direction. The implication here is that the inner cavity has dimensions b and c. We consider the particular cavity which is defined by the values $d = 0.2\lambda = 0.2$, $b = 4\lambda = 4$ and $c = \lambda = 1$. A hybrid unstructured mesh is constructed to solve the problem, an illustration of which can be found in Figure 9 (a). In Figures 9 (c) and (d) we present the scattering width distributions obtained for waves with incident directions $\theta = 0$ and $\theta = 45$ degrees. In both cases we compare the results with that of the hp–version approach. For the incident direction of $\theta = 0$ we observe a very good agreement in the scattering width distribution. Although for the case of the incident direction $\theta = 45$ the plane wave approach exhibits some differences to the hp approach. However, the results still remain very similar. In Table 4 we show a comparison of the

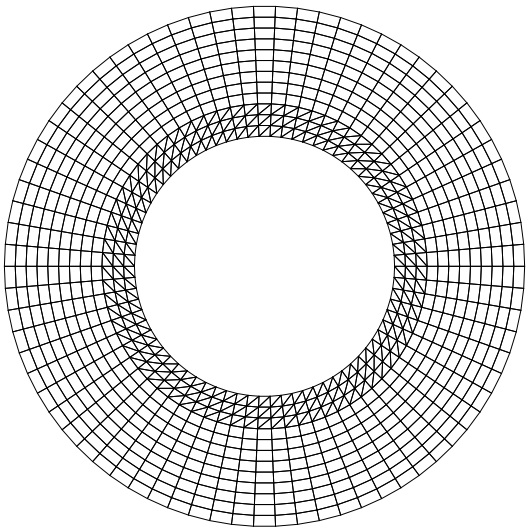

(a)

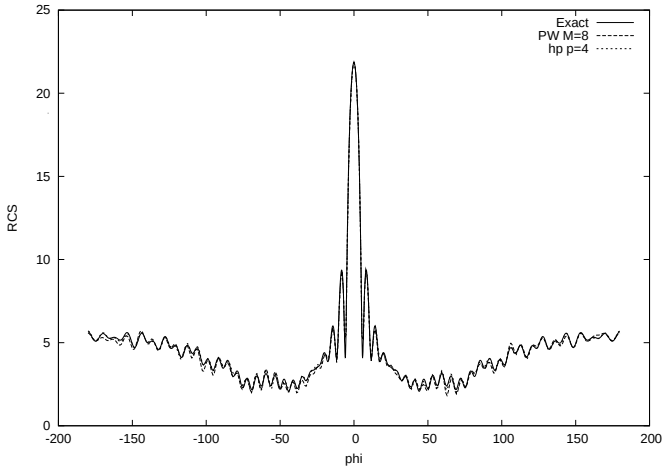

(b)

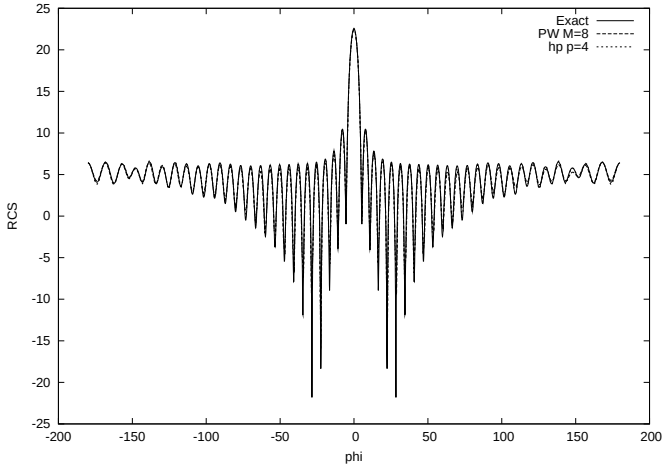

(c)

Figure 8: Scattering by a coated cylinder of electrical length 8λ showing: (a) a mesh with $3\text{pts}/\lambda$, (b) PEC scattering width distribution and (c) PMC scattering width distribution.

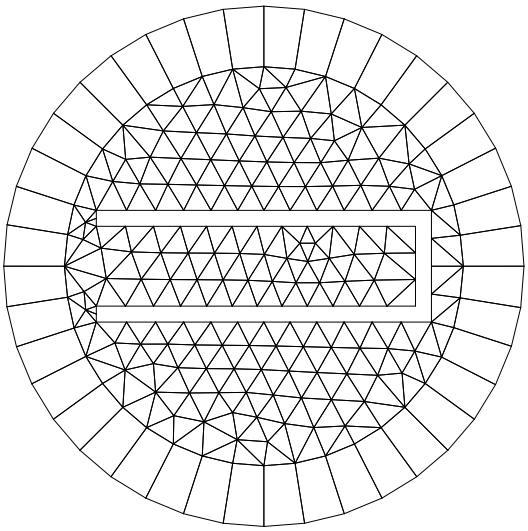

(a)

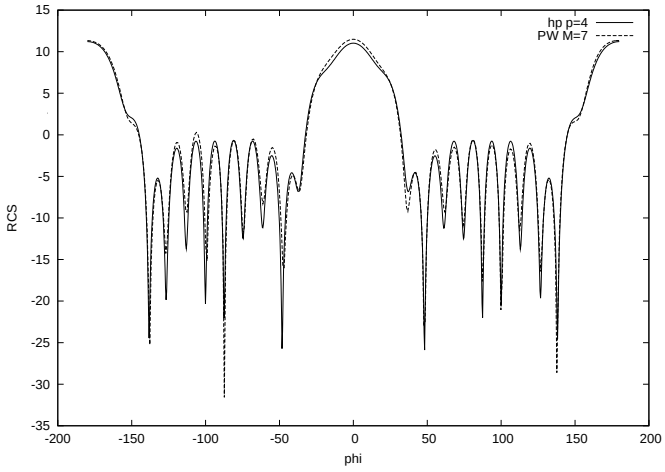

(b)

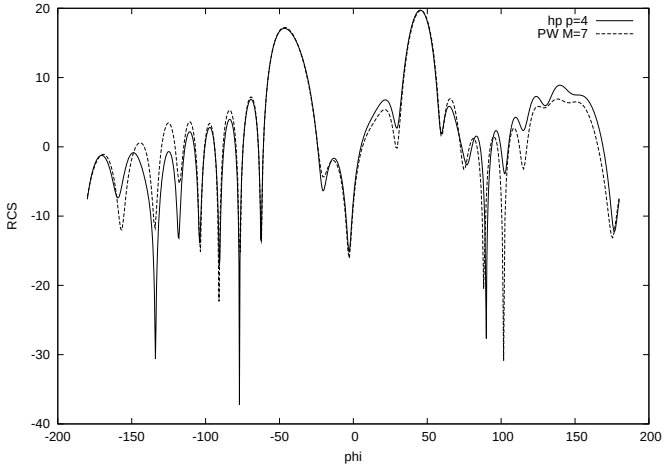

(c)

Figure 9: Scattering by a U shaped cavity rotated through 90 degrees, of electrical length 4λ showing: (a) a mesh with 3pts/λ, (b) PEC scattering width distribution for $\theta = 0$ and (c) PEC scattering width distribution for $\theta = 45$.

	Total Unknowns	Linear Solver Dimension	Bandwidth
hp–version PEC	9335	3010	305
PW version PEC	4002	4002	427

Table 4: Comparison of the number of unknowns required by the PW version and *hp*–version $\boldsymbol{H}(\text{curl})$ conforming finite element methods in order to obtain comparable accuracy for a coated 4λ cavity.

computational resources required for the 4λ cavity example.

Next we consider scattering by a NACA0012 aerofoil. We consider electrical lengths λ and 2λ, but use the same mesh for both cases. The unstructured hybrid mesh employed is shown in Figure 10 (a). The implication for this example is that the number of points per wavelength is reduced for the larger electrical length. The mesh is generated in such a way that a small mesh spacing appears in the neighbourhood of the leading and trailing edges where singularities are known to exist. It is hoped that this specially designed mesh will improve the handling of the singularities. In Figure 10 (b) and (c) we show the scattering width distributions obtained for the electrical lengths λ and 2λ when an incident wave with the direction $\theta = 0$ is considered. In both cases the agreement between the plane wave and *hp* approaches is very good.

In Table 5 we show a comparison of the computational resources required for the plane wave and *hp* approaches. Note that for the plane wave approach we select $M_{max} = 6$ for both electrical lengths. Due to the adaptive way in which the directions are selected, the number of allowable directions on the smallest triangular elements increases with the frequency. This is because the elemental condition number for these elements reduces as the number of points per wave length increases. We therefore observe an increase in total number of unknowns for the plane wave approach, as shown in Table 5 . For the *hp* approach a higher degree polynomial is required for the 2λ example, thus resulting in the increase in number of degrees of freedom for this case.

	Total Unknowns	Linear Solver Dimension	Bandwidth
hp–version λ	11392	4608	572
PW version λ	5327	5327	858
hp–version 2λ	26544	6912	858
PW version 2λ	6762	6762	858

Table 5: Comparison of the number of unknowns required by the PW version and *hp*–version $\boldsymbol{H}(\text{curl})$ conforming finite element methods in order to obtain comparable accuracy for NACA0012 aerofoils of electrical lengths λ and 2λ .

7 Conclusions

In this report we have extended our previous work on plane wave $\boldsymbol{H}(\text{curl})$ conforming elements [20] to electromagnetic scattering problems. Methods have been proposed for the application of Dirchlet and Neumann boundary conditions together with a new approach which leads to the accurate evaluation of the scattering width output. Results on both quadrilateral and hybrid meshes demonstrate that the proposed method is very accurate at predicting the scattering width distributions for coated and uncoated PEC and PMC cylindrical scatterers. The method also compares well with a *hp* code for non–cylindrical scatterers. Comparisons of the computational cost of the method with that of the *hp* approach demonstrate that the required number of global unknowns is smaller. On going research is concentrated in to the efficient selection of the directions, which it is hoped will lead to a reduction in the size of the linear system for the plane wave approach.

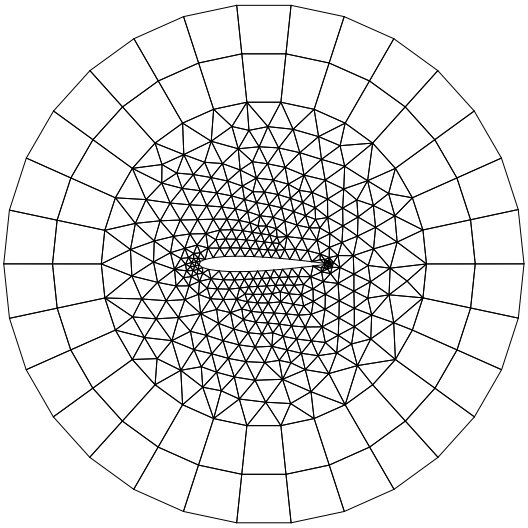

(a)

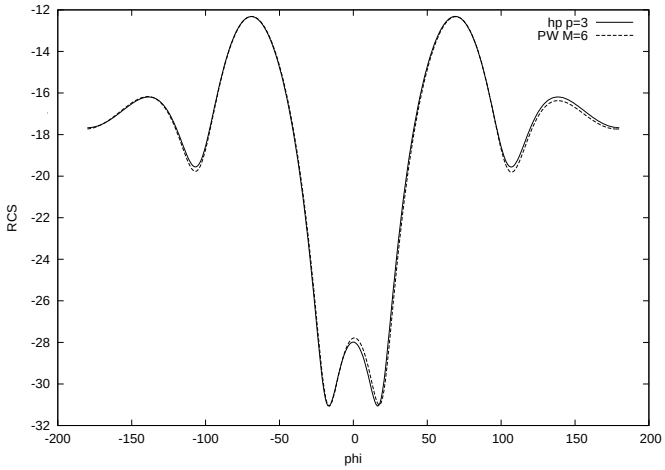

(b)

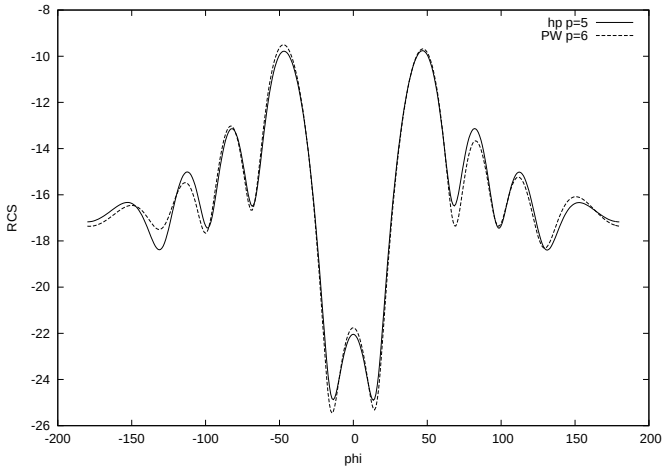

(c)

Figure 10: Scattering by a NACA0012 aerofoil for incident waves with $\theta = 0$ showing: (a) a hybrid mesh with variable spacing, (b) PEC scattering width distribution for electrical length λ and (c) PEC scattering width distribution for electrical length 2λ .

A Plane wave approach for dielectric media

In this report we postulated that the scattered field in air may be written as

$$\boldsymbol{E}_H^s = \sum_{n=1}^{N} \boldsymbol{\phi}_n \sum_{m=1}^{M(n)} A_n^m \exp\{\mathrm{i}\omega(x\cos\theta_m + y\sin\theta_m)\} \tag{59}$$

where N is the total number of basis functions. We now wish to explore this approximation in a little more detail, for the case of dielectric mediums.

Following Jackson [13], let us consider a dielectric interface between two materials, as shown in Figure 11 the first with properties ϵ and μ, the second with properties ϵ' and μ'. We consider a wave incident to this interface and examine the resulting transmitted and reflected waves

- Incident wave
$$\boldsymbol{E}^k = \boldsymbol{E}_0 \exp\{\mathrm{i}\boldsymbol{k}\cdot\boldsymbol{x}\} \tag{60}$$
- Transmitted wave
$$\boldsymbol{E}^{k'} = \boldsymbol{E}_0' \exp\{\mathrm{i}\boldsymbol{k}'\cdot\boldsymbol{x}\} \tag{61}$$
- Reflected wave
$$\boldsymbol{E}^{k''} = \boldsymbol{E}_0'' \exp\{\mathrm{i}\boldsymbol{k}''\cdot\boldsymbol{x}\} \tag{62}$$

In order that the interface conditions (6,7) are satisfied, we require on $y = 0$ that

$$\boldsymbol{k}\cdot\boldsymbol{x} = \boldsymbol{k}'\cdot\boldsymbol{x} = \boldsymbol{k}''\cdot\boldsymbol{x} \tag{63}$$

The amplitudes of the vector wavenumbers $\boldsymbol{k}, \boldsymbol{k}'$ and $\boldsymbol{k}''$ are as follows

$$|\boldsymbol{k}| = |\boldsymbol{k}''| = k = \frac{\omega}{c}\sqrt{\mu\epsilon} \qquad |\boldsymbol{k}'| = k' = \frac{\omega}{c}\sqrt{\mu'\epsilon'} \tag{64}$$

and it follows that

$$k\sin i = k'\sin r = k''\sin r' \tag{65}$$

Further, note that as $i = r'$, then $k = k''$.

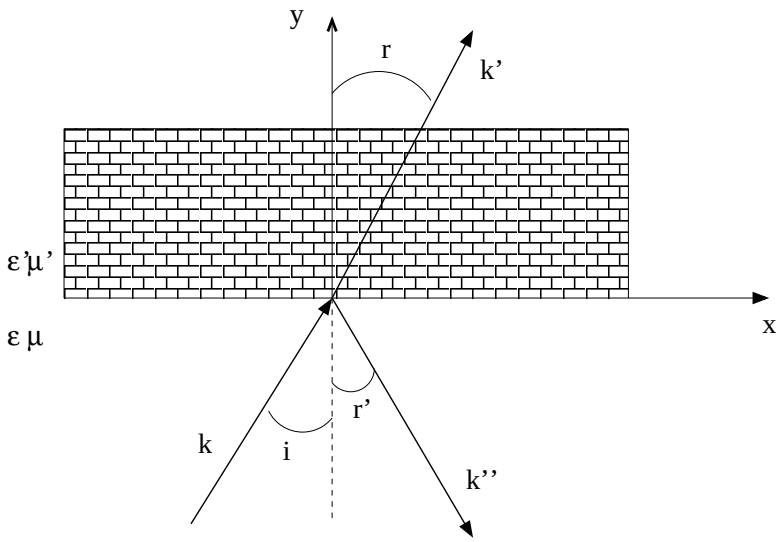

Figure 11: Interface between two materials

Let us now turn our attention to our plane wave finite element procedure in dielectric media. At first sight, one might expect that the field inside the dielectric should be approximated as

$$\boldsymbol{E}_H^s = \sum_{n=1}^{N} \boldsymbol{\phi}_n \sum_{m=1}^{M(n)} A_n^m \exp\{\mathrm{i}k_d(x\cos\theta_m + y\sin\theta_m)\} \tag{66}$$

using the wavenumber in the dielectric, ($\omega^2 = k_d^2\epsilon\mu$) However, we see that this is not necessarily the case.

On a given edge n of the dielectric interface Γ_{12} we prescribe a number of directions $\theta_1, \theta_2, \cdots, \theta_{M(n)}$, which will be the same independent of whether the edge is considered as part of the free space region or as part of the dielectric medium. We require that $\boldsymbol{\tau}\cdot\boldsymbol{E}_H^s|_{fs} = \boldsymbol{\tau}\cdot\boldsymbol{E}_H^s|_d$ on edge n. This then suggests that we should use

$$\boldsymbol{\tau}\cdot\boldsymbol{E}_H^s|_d = C\sum_{m=1}^{M(n)} A_n^m \exp\{\mathrm{i}\omega(x\cos\theta_m + y\sin\theta_m)\} \tag{67}$$

as the approximation of the field on edges adjacent to the dielectric region (when viewed from inside the dielectric). This choice then automatically satisfies equation (63) for all of the considered plane wave directions.

On edges residing in the interior of the dielectric, one may also use the approximation based on the frequency ω as the solution procedure will automatically select the amplitudes A_n^m of the wavenumbers $(\omega\cos\theta_m, \omega\sin\theta_m)$, corresponding to the wavenumber of the wave in the dielectric medium, to have the largest magnitude.

References

[1] M. Ainsworth. Discrete propertiies of high order Nédélec/edge element approximation of the time–harmonic Maxwell equations. *Philosophical Transactions of the Royal Society Serie A*, 362:471–493, 2004.

[2] M. Ainsworth and J. Coyle. Hierarchic *hp*–edge element families for Maxwell's equations on hybrid quadrilateral/triangular meshes. *Computer Methods in Applied Mechanics and Engineering*, 190:6709–6733, 2001.

[3] I. Babuska and J.M. Melenk. The partition of unity method. *International Journal for Numerical Method in Engineering*, 40:727–758, 1997.

[4] I.M. Babuska, F. Ihlenburg, E.T. Paik, and S.A. Sauter. A generalised finite element method for solving the Helmholtz equation in two dimensions with minimal pollution. *Computer Methods in Applied Mechanis and Engineering*, 128:325–359, 1995.

[5] I.M. Babuska and S.A. Sauter. Is the pollution effecit of the FEM avoidable for the Helmholtz equation considering high wave numbers? *SIAM Review*, 42:451–484, 2000.

[6] A. Bayliss and E. Turkel. Radiation boundary conditions for wave–like equations. *Communications in Pure and Applied Mathematics*, 33:707–725, 1980.

[7] J-P Berenger. A perfectly matched layer for the absorption of electromagnetic waves. *Journal of Computational Physics*, 114:185–200, 1994.

[8] P. Bettess. *Infinite Elements*. Penshaw Press, Sunderland, 1992.

[9] P. Bettess, J. Shirron, O. Laghrouche, B. Peseux, R. Sugimoto, and J. Trevelyan. A numerical integration scheme for special finite elements for the helmhotz equation. *International Journal of Numerical in Engineering*, 56:531–552, 2003.

[10] W. Cecot, L. Demkowicz, and W. Rachowicz. A two dimensional infinite element for Maxwell's equations. *Computer Methods in Applied Mechanics and Engineering*, 188:625–643, 2000.

[11] R. Hiptmair. Coupling of finite elements and boundary elements in electromagnetic scattering. *SIAM Journal of Nuermical Analysis*. accepted.

[12] R. Hiptmair and P.D. Ledger. A quadrilaterial edge element scheme with minimum dispersion. Technical Report 17, Seminar for Applied Mathematics ETH Zürich, 2003.

[13] J.D. Jackson. *Classical Electrodynamics*. Wiley, 1975.

[14] M. Kuzuoglu and R. Mittra. Investigation of nonplanar perfectly matched absorber for finite element mesh truncation. *IEEE Transactions on Antennas and Propagation*, 45:474–486, 1997.

[15] O. Laghrouche and P. Bettess. Short wave modelling using special finite elements. *Journal of Computational Acoustics*, 8:189–210, 2000.

[16] O. Laghrouche, P. Bettess, and R.J. Astley. Modelling of short wave diffraction problems using approximating systems of plane waves. *International Journal for Numerical Methods in Engineering*, 54:1501–1533, 2002.

[17] P.D. Ledger. *An hp-Adaptive Finite Element Proceedure for Electromagnetic Scattering Problems*. PhD thesis, Dept. Civil Engineering, University of Wales, Swansea, 2002.

[18] P.D. Ledger and K. Morgan. The application of the *hp*–finite element method to electromagnetic problems. *Archives of Computational Methods in Science and Engineering*, 2004. submitted.

[19] P.D. Ledger, K. Morgan, O. Hassan, and N.P. Weatherill. Arbitrary order edge elements for electromagnetic scattering simulations using hybrid meshes and a PML. *International Journal for Numerical Methods in Engineering*, 55:339–358, 2002.

[20] P.D. Ledger, K. Morgan, O. Hassan, and N.P. Weatherill. Plane wave $\boldsymbol{H}$(curl) conforming finite elements for Maxwell's equations. *Computational Mechanics*, 31:272–383, 2003.

[21] P.D. Ledger, J. Peraire, K. Morgan, O. Hassan, and N.P. Weatherill. Efficient highly accurate *hp*-adaptive finite element computations of the scattering width output of Maxwell's equations. *International Journal for Numerical Methods in Fluids*, 43, 2003.

[22] J.M. Melenk and I. Babuska. The partition of unity finite element method: basic theory and applications. *Computer Methods in Applied Mechanics and Engineering*, 139:289–314, 1996.

[23] P. Monk. The near to far field transformation. *COMPEL The International Journal for Computation and Mathematics in Electrical and Electronic Engineering*, 14:41–56, 1995.

[24] P. Monk, T. Huttunen, and J.P. Kaipio. Computational aspects of the ultra weak variational formulation. *journal of Computational Physics*, 182:27–46, 2002.

[25] P. Monk and E. Suli. The adaptive computation of far field patterns by a posteriori error estimation of linear functionals. *SIAM Journal of Numerical Analysis*, 36:251–274, 1998.

[26] G. Mur. Edge elements, their advantages and their disadvantages. *IEEE Transactions on Magnetics*, 30:3552–3557, 1994.

[27] J.C. Nédélec. Computation of Eddy currents on a surface in $\mathbb{R}^3$ by finite element methods. *SIAM Journal of Numerical Analysis*, 15:580–594, 1978.

[28] J.C. Nédélec. Mixed elements in $\mathbb{R}^3$. *Numerische Mathematik*, 35:315–341, 1980.

[29] J.C. Nédélec. A new family of mixed elements in $\mathbb{R}^3$. *Numerische Mathematik*, 50:57–81, 1986.

[30] J.A. Stratton. *Electromagnetic Theory*. McGraw–Hill, 1941.

[31] D. Sun, J. Manges, X. Yuan, and Z. Cendes. Spurious modes in finite-element methods. *IEEE Antennas and Propagation Magazine*, 37:12–24, 1995.

[32] B. Szabo and I. Babuska. *Finite Element Analysis*. John Wiley and Sons, 1991.

[33] G.S. Warren and W.R. Scott. An investigation of the numerical dispersion in the vector finite element method using quadrilateral elements. *IEEE Transactions on Antennas and Propagation*, 42:1502–1508, 1994.